Analogue signaling of somato-dendritic synaptic activity to axon enhances GABA release in young cerebellar molecular layer interneurons

Federico F. TRIGO[1*†] and Shin-ya KAWAGUCHI[2*]

[1]Departamento de Neurofisiología Celular y Molecular, Instituto de Investigaciones Biológicas Clemente Estable, Avenida Italia 3318, Montevideo 11600, Uruguay.

[2]Department of Biophysics, Graduate School of Science, Kyoto University Oiwake-cho, Kitashirakawa, Sakyo-ku, Kyoto, 606-8502, Japan.

* Corresponding authors.

[†] Lead contact.

Summary.

Analogue signaling is the phenomenon by which subthreshold activity in the dendrites and soma of neurons is transmitted down the axon. Although it has been demonstrated in many different preparations, the extent and physiological role of analogue signaling for subthreshold, somatodendritic spontaneous activity have not been studied in detail. In order to address this we performed simultaneous, whole-cell recordings of the soma and axon of young cerebellar interneurons. We show that the somatodendritic spontaneous glutamatergic events are transmitted down the axon for significant distances and produce a measurable change in the voltage of the axonal varicosities. By combining electrophysiological recordings in the culture preparation and in slices, we further show that the analogously transmitted EPSPs can affect GABA release significantly, and that this effect is not due to a modification in the axonal AP shape or amplitude.

Introduction.

Analogue signaling, the phenomenon by which somatodendritic subthreshold neuronal activity is transmitted to the axon, has been described in a variety of different preparations in mammals (for an exhaustive, recent review, see[1]). However, the quantification of the coupling with direct, simultaneous electrophysiological soma-axon recordings has been scarce in the literature, probably because of the difficulties in recording from small varicosities of an intact axon arising from the soma in the majority of experimental preparations. As a corollary, analogue signaling has usually been studied only for long (hundreds or thousands of ms), depolarizing or hyperpolarizing voltage changes, and the incidence, extent and physiological role of analogue signaling for subthreshold spontaneous activity is only known in a handful of neuronal types[2–4]. Direct axonal patch-clamp recordings have shown, both in the hippocampal mossy fiber > CA3 synapse[2] and in synapses between layer 5 pyramidal cells[3], that subthreshold spontaneous or evoked somatodendritic activity can reach the axon. In cerebellar molecular layer interneurons (MLIs), on the other hand, previous data obtained by paired recordings from pre- and postsynaptic soma suggest that subthreshold coupling between the somatodendritic and axonal compartments is also substantial[5–9], even for spontaneous activity[10,11].

Cerebellar MLIs allow to quantitatively study the extent and functional impact of analogue signaling because their axonal bouton can be directly recorded with the patch-clamp technique, as shown by Southan and Robertson[12–14] in pioneering, *tour-de-force* experiments. In the present work we performed for the first time simultaneous electrophysiological, whole-cell patch-clamp recordings from the soma and the axon of cerebellar MLIs in order to assess the coupling under

regimes of physiological activity and understand its physiological role. We quantitatively show that in young MLIs (PN 13 to 17) the analog coupling of somato-dendritic synaptic activity to axon is substantial. We further show that this spontaneous synaptic activity coupling can affect transmitter release through a mechanism that involves a modulation of voltage-dependent calcium channels, with no change in the presynaptic AP waveform or basal calcium. Our findings highlight the importance of subthreshold coupling between neuronal compartments and add yet another mechanism by which analog coupling can modulate synaptic transmission.

Results.

In order to assess directly the degree of coupling between the somatodendritic and the axonal compartments we performed paired whole-cell recordings (WCR) from the soma and the intact axonal varicosities of cerebellar MLIs in an acute slice at near physiological temperature (34 °C). To do so we first patched the somatic compartment with an intracellular solution (IS) containing the fluorescent dye Alexa 594; after waiting for a few minutes for the dye diffusion we went on to patch an axonal varicosity with a pipette containing the same IS without Alexa. In the example shown in **figure 1A** the distance between the center of the soma and the selected axonal varicosity is 150 µm (magenta line; minimum and maximum recording distances from the soma: 64.5 and 244 µm, respectively). **Figure 1B** shows a picture (the dotted rectangle in **A**) of the recording configuration during the cell-attached mode, a few seconds before rupturing the patch, and **figure 1C** the same picture a few seconds after break-in (the intra-varicosity fluorescence disappears immediately after break-in). The bottom traces in **figure 1B** and **C** show the orthodromically transmitted axonal action potentials (axAPs) recorded in different configurations after inducing a somatic spike: in cell-attached (**1B**); an unclamped spike current in voltage-clamp (VC) and a short train of APs recorded in current-clamp (CC; **1C**).

To quantify the coupling for spontaneous synaptic activity we performed two types of experiments. In the first, we recorded spontaneous excitatory synaptic potentials (sEPSP) in paired, somato-axonal, recordings. **Figure 2A** shows the recording configuration (**top**) and transmitted and fluorescent light pictures of the recorded axonal varicosity (**bottom**; which in this case was contacting a Purkinje cell soma). As can be seen in **figure 2B**, the simultaneous CC recordings from the soma and the axon shows that every somatodendritic sEPSP is accompanied by the almost coincident appearance of an EPSP in the axonal varicosity (located here at 111.75 µm from the soma). These axonal EPSPs are smaller in amplitude (mean ± SD amplitude of somatic and axonal EPSPs in this cell: 13.1 ± 2.0 mV and 7.8 ± 1.6 mV, respectively; n = 29 events, 50 s recording time, with an average coupling ratio [CR; see methods] of 0.6 ± 0.07), have a longer risetime (mean ± SD 10-90% risetimes of somatic and axonal EPSPs: 1.8 ± 0.49 ms and 5.7 ± 1.6 ms, respectively) and always appear later than the somatically recorded EPSPs (lag in the cross-correlation between the somatic and axonal recordings: 2.33 ms; **figure 2D**). All of these data indicate that the somatically recorded EPSPs are closer to the source of current, namely the dendritic postsynaptic densities, and are compatible with classical cable models for the propagation of subthreshold events in neuronal compartments. The analysis of the decaying phase of the axonal and the somatic events shows that the axonal EPSP decay is well fitted with a mono-exponential function with a tao (20.4 ±

0.021 ms) which is extremely close to the slower time constant, τ2, of the somatic EPSP average (19.9 ± 0.02). This (the fact that the final phase of decay ,τ2, of the somatic and the axonal events is the same) is also predicted by cable models, which indicate that the decay cannot be slower than the membrane time constant of the cell[15].

In the second type of experiment we performed spot laser photolysis of MNI-glutamate[16,17]. **Figure 2E** shows the recording configuration: MNI-glutamate was photolysed in 7 different dendritic varicosities plus the soma (**figure 2E**; magenta spots). The laser-evoked EPSPs (eEPSPs) recorded simultaneously from the soma and the axon are shown in **figure 2F**. As shown in **figure 2G**, the soma-axon CR for eEPSPs at the different dendritic varicosities (and the soma) was not affected by the location of glutamate inputs at dendrites. The average CR (dotted line) was 0.4 ± 0.05 (mean ± SD). As a comparison, the DC CR (resulting from 400 ms current injections in the soma) in this cell was 0.71 (not shown). **Figure 2H** shows the amplitude of the somatically recorded dendritic EPSPs as a function of distance. It can be seen that the higher amplitude is obtained when glutamate is photolysed at the farthest varicosity (and the lower amplitude when it is photolysed at the soma) which indicates that the amount of dendritic filtering in young MLIs is not prominent and that the number of postsynaptic glutamate receptors is probably larger at distant dendrites. In summary, glutamate photolysis in MLI dendrites to mimic sEPSPs confirms that synaptic events at dendrites can travel long distances down the axon.

We next quantified the distance-dependence of the somato-axonal EPSP coupling by measuring the EPSP CR as a function of distance (**figure 2I**; both spontaneous and laser-evoked EPSPs were used for the analysis). The length constant, λ, of this distance-dependent relationship is 178 ± 15 µm, which indicates that the analog coupling between the somatodendritic and axonal compartments in young MLIs is prominent for synaptic activity.

The experiments presented so far indicate that in physiological conditions MLI axonal varicosities, where transmitter release happens, are then exposed to similar voltage fluctuations than the soma. Because previous studies from our and other laboratories have shown that analog signaling for long (> hundreds of ms) depolarizing pulses can affect release, we wondered whether the analogically traveling spontaneous synaptic activity could affect release as well. In order to test this possibility we turned to the primary cerebellar culture preparation, where interneurons can be sparsely infected with an adeno-associated virus (AAV) that drives the expression of eGFP. This allows to do

simultaneous recordings of a single MLI axonal varicosity and its postsynaptic cell and hence to perform a detailed analysis of the release at the synapse.

In order to test whether small depolarizations similar to spontaneous EPSPs can affect release we performed paired recordings of a single varicosity and its postsynaptic partner. The presynaptic varicosity was voltage-clamped with a voltage waveform that consisted of either a single AP (**figure 3A**, black, left traces) or an AP preceded by two consecutive EPSPs (**figure 3A**, brown, right traces; for details see methods and **supplementary figure 1**). Upon the application of a realistic stimulus, the control AP waveform, a preICa^{++} is induced that triggers a PSC (**figure 3A**). When the AP is preceded by the EPSPs the corresponding preICa^{++} is larger and so is the PSC. **Figure 3B** depicts the temporal relationship of the onset (dotted line "a") and the peak (dotted line "b") of the preICa^{++} in relation to the AP, which shows that the difference between the calcium currents in both conditions does not appear at the onset but at the peak of the current, during the decaying phase of the AP. **Figure 3C** shows the relative increases (AP waveform with over without depolarization) of the preICa^{++} and PSC amplitude, that are both significant.

During the course of our experiments we also patched a cerebellar granule cell terminal contacting a MLI. The same experiments performed in such a pair did not show any increase in the preICa^{++} nor PSC amplitude (**supplementary figure 2A**).

The above experiments show that even short, PSP-like voltage fluctuations in the axonal varicosity right before the AP can modulate release. In order to understand the mechanism by which the preAP potential modulates the ICa^{++} amplitude we performed the following experiments. First, we recorded the ICa^{++} in a bouton upon depolarizing pulses in order to explore the characteristics of the current in terms of kinetics and activation voltage. When the terminal is voltage-clamped to 0 mV for various durations, an inward ICa^{++} develops with an activation time constant of around 3.0 ms and little or no inactivation (**Figure 3D**; n = 15). On the other hand, as shown in **Figure 3E**, the IV curve (from a total of 16 varicosities: 12 varicosities from primary cultures and 4 from slices) indicates that the take-off of the ICa^{++} is variable but always more depolarized than -40 mV, so it is unlikely that small depolarizations like the ones induced by sEPSPs would directly open the calcium channels. There still exists the possibility that very small calcium currents may not be detected because buried into the recording noise. To test for this possibility we analyzed the current variance (the variance is proportional to the number of open channels[18,19]) in presynaptic recordings at -70 mV and during depolarizations to -40 mV (the maximal depolarization tested; **Figure 3F**).

This analysis shows that the variance during these 2 time epochs is the same, which is in agreement with the activation voltage shown on the IV curve before. These experiments confirm that the preAP depolarizations do not open the Ca^{++} channels. Therefore, the mechanism by which the preAP depolarization augments $preICa^{++}$ and transmission does not involve any direct activation of Ca^{++} channels in a bouton.

To gain a better understanding of the relationship between the subthreshold potential and release, we performed a similar type of experiment to the one presented in **Figure 3A**, but now the $preICa^{++}$ (and release) was triggered by a square depolarization (to 30 mV) preceded by 20 ms depolarizations to different voltages (-90 to -40 mV). **Figures 3G** and **H**, left, show that the $preICa^{++}$ (and the subsequent PSC) is highly dependent on the subthreshold voltage before the suprathreshold pulse: the more depolarized is the preVm, the larger are the $preICa^{++}$ and subsequent release. A complete statistical analysis of the responses induced by the different prepulses is shown in **supplementary figure 3**, where the responses ($preICa^{++}$ and PSC) obtained with the different prepulses were compared between each other. Again, there is no evidence of any activation of the $preICa^{++}$ during the subthreshold depolarization. When a 5 ms interval is added before the suprathreshold pulse, the preceding subthreshold voltage levels do not have any influence on the $preICa^{++}$ (**Figure 3G**, and **3H,** right). This has mechanistic implications that will be discussed below. When the same protocol was applied to the granule cell terminal, there was no change in either of the 2 amplitudes ($preICa^{++}$ or PSC; **supplementary figure 2B**).

In the final series of experiments we turned again to the slice preparation in order to assess whether these short, preAP, subthreshold depolarizations can change release as was shown in the culture preparation. In order to do this we performed paired whole-cell recordings between MLIs and the postsynaptic Purkinje cells. Alexa 594 fluorescent dye was included in the IS to allow for MLI visualization (**Figure 4A**). Once a connection was established, the MLI was held in VC and two types of interleaved protocols applied: the control one consisted of a train of 5 stimuli (depolarization to 0 mV for 2 ms at 30 Hz) in order to induce somatic spikes; the test one was identical but the 1st AP inducing pulse was preceded by a short (20 or 50 ms), subthreshold depolarization of presynaptic MLI soma, similar to the one presented in **Figure 3G**. From the PSC train (**Figure 4B**), we quantified both the PSC amplitude of the first response (**Figure 4C**) and the amplitude ratios of the subsequent PSCs in the train (**Figure 4D**). When the AP is preceded by a subthreshold depolarization the PSC amplitude is bigger than without the subthreshold depolarization. Also, there is a decrease in the amplitude of subsequent PSCs, which reflects an

increase in the release probability at the 1st stimulation and a lower availability of release-competent vesicles at the subsequent stimuli. These results indicate that short, somatically applied subthreshold depolarizations right before the AP can increase release, as revealed by an increase in PSC amplitude and the resultant decrease of later release.

By controlling the gating of presynaptic calcium channels, the duration of the axAP has a strong impact on the amount of released neurotransmitter[20,21]. In cerebellar MLIs, the modulation of the axAP duration has been shown to happen as a result of analog transmission from the somatodendritic compartments[8,9]. The results presented here (**Figure 3**) indicate that transmitter release from MLI terminals can be modulated by a subthreshold potential change even in the absence of any change in the axAP width. In order to confirm this idea, after finishing the experiment presented in **Figure 4A** to **4D**, we attempted to patch the presynaptic MLI axonal varicosity that was tentatively contacting the postsynaptic Purkinje cell. In order to do that the postsynaptic Purkinje cell pipette was removed and replaced by a smaller-tip electrode in order to perform a cell-attached recording of APs from the presynaptic cell axon. **Figure 4E** shows an example. We then applied the same (control and test) protocols as described in the previous paragraph. Under these conditions, the axAP width remained unchanged between the control and test protocols (**Figure 4F** and **G**, **left**; 4 recordings with prior postsynaptic Purkinje cell recordings and 8 recordings where only soma-axon recordings were performed). The first AP amplitude, on the other hand, showed a small, although significant, decrease (8%; **Figure 4G**, **right**), which is probably due to a decrease in the driving force for sodium influx during the AP onset because of the somatically-elicited depolarization arriving to the varicosity. These experiments indicate that the change in synaptic efficacy found in the slice preparation does not involve any change in the axAP width. More generally, both the width and the amplitude of the axonal APs recorded in the cell-attached mode in somato-axonal pairs were extremely stable, as shown in detail in **Supplementary information** and **supplementary figure 4**, indicating that the axAP in MLIs is not particularly susceptible to activity-dependent modifications.

Discussion.

In this work we performed for the first time simultaneous WCRs of the soma and axonal varicosities of cerebellar MLIs. These experiments allowed us to measure directly the synaptic activity coupling between the 2 compartments. As anticipated from previous works with other methods (Ca^{++} imaging[6,7], Ca^{++} and GABA photolysis[11], voltage-sensitive dye imaging[8] and electrophysiology[5,10]), we show here that the subthreshold voltage coupling in animals aged 12 to 17 days old is highly prevalent in these cells, even for short, subthreshold spontaneous activity (ie: EPSPs). We further show that the EPSPs that reach the axon can modulate release through a mechanism that is independent from any change in basal calcium or AP waveform.

The mechanism by which orthodromic EPSP coupling affects release.

It has been shown before by multiple groups, in cerebellar MLIs and in other neuronal types, that the somato-dendritic membrane potential can be transmitted down the axon and affect transmitter release through the modulation of voltage-dependent conductances[1]. This may be due to a change in the AP waveform (amplitude and/or duration[3,8]), a change of basal calcium concentration[6,7] or to other, non-defined mechanisms[2,22]. The term analog-digital transmission is used to stress the fact that the subthreshold voltage (the analog signal) before the arrival of the AP (the digital signal) can affect release. The results presented here show that: a) the modulation of release does not require long or large voltage changes, but short and small, PSP-like voltage fluctuations of ≈ 10 mV can affect release; b) the mechanism involved does not include any change in the preAP waveform or in the presynaptic Ca^{++} influx right before the arrival of the AP. Even in these conditions, the subthreshold depolarization before the AP does induce an increase in the Ca^{++} influx during the AP and hence an increase in release. Our results are compatible with the following interpretation: during the subthreshold depolarization there is an increase in the voltage-dependent probability of the 4 voltage sensors of the Ca^{++} channels to go from the “resting-down” to the “activated-up” position[23], but the pore of the channel remains closed. Once the AP is triggered, a bigger fraction of the voltage-gated Ca^{++} channels opens in relation to the control (no preAP depolarization) condition, where the probability of the voltage sensors to be in the activated position is at its minimum. The disappearance of the effect by a 3 to 5 ms interval after the subthreshold depolarization (**Figure 3G** and **H**) is compatible with this idea. In this sense, the mechanism described in this article constitutes, to the best of our knowledge, a new way by which somato-axonal analog coupling can modulate release. At the same time, this work highlights the importance of performing direct axonal recordings in order to study AP propagation and release in CNS axons.

Diverse analog-digital coupling mechanisms in MLIs.

Subthreshold coupling between the somatic and axonal compartments in MLIs was described in the 90s by Glitsch and Marty[24], who showed that long somatic depolarizations can increase GABA release through a pure analog transmission mechanism (similar to what happens in retinal amacrine cells). In 2011, Christie et al.[6] and Bouhours et al.[7] described for the first time an orthodromic subthreshold coupling in MLIs by which somatically-induced depolarizations are transmitted down the axon and increase AP-evoked release through an augmentation in basal calcium, the so-called "analog-digital" transmission mechanism. It was later shown by Rowan and Christie[9] that the analog-digital increase in GABA release is dependent on a modulation of the axonal AP width because of the inactivation of a K conductance (K_V3). This is different from what was found by Bouhours et al., who showed that the analog-digital coupling was dependent on the activation of PKC. In a recent work, Blanchard et al.[25] showed that the modulation of basal calcium with local calcium photolysis in a single MLI axonal varicosity can increase release through a modulation of the docking site occupancy. In the present work, both the amplitude and the half-width of the axAP seem to be very resistant to various manipulations, like an increase in the stimulation frequency (**supplementary figure 4**) and somatic depolarization (**Figure 4**), which is in agreement with what has been described by Alle and Geiger (see above) and by Ritzau-Jost et al.[26], who showed that in neocortical (L5) fast-spiking GABAergic cells the width of the axAP does not change when the stimulation frequency increases. The fact that in our experiments the axAP width does not change, even when short prepulse depolarizations are applied before the AP (**figure 4**), is in contrast to what has been found by Rowan and Christie[9], who showed that somatic preAP depolarizations slow down the axonal AP. The difference may be due to a species difference (rat here vs mice in their work) or to the fact that the applied preAP depolarizations are longer in their article than those applied here.

In MLIs, it seems plausible that multiple mechanisms by which somato-axonal coupling affects release coexist, each one of them probably being initiated under a particular condition (for example, duration and amplitude of the somatic voltage changes). In this sense, it is interesting to note that the kinetics of the presynaptic ICa^{++} is slow (τ around 3 ms, **Figure 3D**). As a comparison, the ICa^{++} opens with an activation time constant of ~ 1 ms in Purkinje cell presynaptic boutons[27] and ~ 2 ms in cerebellar granule cells[28]. This slow time constant of Ca++ channel activation in MLI boutons does not seem to be due to poor voltage clamp conditions. If this was the case, one would expect a correlation between the measured time constant and the Rs values: the higher the Rs, the slower the τ. However, no correlation was found between the τ and Rs values measured from the 16 different

varicosities presented in **Figure 3D**. From the average Rs value calculated from those varicosities (83 MΩ), on the other hand, an approximate voltage clamp time constant of 200 µs can be calculated, assuming a varicosity capacitance of 1 to 2 pF. In summary, the slow τ of the ICa^{++} indicates that a very small fraction of the available Ca^{++} channels opens upon the arrival of an AP in MLIs, leaving a big verge for different modulation mechanisms to occur. Indeed, unlike MLI boutons, a cerebellar granule cell bouton does not show an augmentation of $preICa^{++}$ and transmission upon pre-pulse depolarization before AP (**Supplementary figure 2**).

Acknowledgments.

We would like to thank Alain Marty for the critical reading of the manuscript. FFT's work is supported by the ANR (JCJC Grant, ANR-17-CE16-0011-01) and IBRO (Return Home Fellowship to Federico F. Trigo). SK is supported by the Japan Society for the Promotion of Science (Core-to-Core Program A, Advanced Research Networks; KAKENHI grants 22H02721 and 22K19360), the Takeda Science Foundation, and the Naito Foundation.

Author contributions.

FFT and SK contributed equally to this work. Correspondence should be addressed to either of the two authors.

Declaration if interests.

The authors declare no competing interests.

Figure legends.

Figure 1 legend.

A. Fluorescence image of the recorded MLI. The patched varicosity is located at 150 µm from the soma. The position of the axonal patch pipette is represented with dotted yellow lines and the main axon in magenta.

B, C. Top. Simultaneous transmitted and fluorescent light pictures of the area shown with the dotted rectangle in **A**, which shows the recorded axonal varicosity before (**B**) and after (**C**) rupturing the seal. In **B**, the fluorescence image is saturated and does not reflect the real size of the varicosity. **Bottom.** Somatic (upper) and axonal (lower), voltage- (left) or current-clamp recordings (right) of somatically induced Na^+ current (or action potentials) and its propagation to the varicosity.

Figure 2 legend.

A. Top. Recording configuration. **Bottom.** Pictures highlighting the position of the recorded axonal varicosity on top of a Purkinje cell somata during the cell-attached configuration. The inset shows an expanded view of the varicosity showing the fluorescence inside the patch pipette.

B. CC recordings of spontaneous synaptic activity in the soma and the axon of the MLI. Resting membrane potential is indicated on top of each trace.

C. Two selected time epochs are shown (**a** and **b** in **B**) with an expanded time-scale.

D. Cross-correlogram of the traces shown in **B**.

E. Fluorescent picture of an Alexa 594-filled MLI showing the experimental configuration. Glutamate was photolysed from MNI-glutamate at different dendritic varicosities (magenta spots 1 to 7 plus soma) while simultaneously recording from the soma and axon. The inset, which corresponds to a single picture, shows that all the dendritic varicosities tested are at the same depth.

F. Somatic and axonal CC recordings of the depolarizations evoked by the photolysis of glutamate at the different varicosities (and soma) shown in **E**. Brown dots indicate the timing of the laser pulse. Laser pulse duration and power are 100 µs and 2 mW, respectively.

G. CR between the soma and axon for each tested dendritic varicosity as a function of distance of the stimulated site to the soma. Dotted line is the average.

H. Somatically recorded eEPSP amplitude as a function of distance.

I. EPSPs amplitude ratios as a function of distance between somatic and axonal recording sites. The continuous line shows the fit with an exponential function. Data include experiments with sEPSPs and eEPSPs. Individual points correspond to the average ratio calculated from the average of all the detected EPSPs in each cell

Figure 3 legend.

A. Simultaneous, VC recording of a presynaptic varicosity and the postsynaptic cell. Upper traces show the voltage waveforms applied, middle traces the recorded preICa^{++} and bottom traces the PSC.

B. Expanded AP waveforms (upper traces) and the resulting preICa^{++} (bottom traces). The "a" and "b" dotted lines correspond to the onset and peak of the preICa^{++}, respectively.

C. Relative increases (waveform with EPSPs over that without EPSPs) of the preICa^{++} (**left**; 1.24 ± 0.25, n = 9, $p < 0.05$) and PSC (**right**; 1.58 ± 0.46, n = 6, $p < 0.05$) amplitudes.

D. Top. VC recordings showing representative traces of preICa^{++} upon depolarization to 0 mV for various durations (1, 2, 5, 10, 20 and 50 ms).

Bottom. Average preICa^{++} as a function of stimulus duration (mean ± SEM. Red line is the fit to the data with an exponential function. Number of boutons analyzed: 1 ms = 4; 2 ms = 8; 5 ms = 12; 10 ms = 16; 20 ms = 16; 50 ms = 16.

E. Current to voltage relationship of the preICa^{++} (mean ± SD; n = 16).

F. Top. Representative preICa^{++} (upper traces) and the corresponding VC protocol (lower trace). The variance was measured in the time epochs indicated by the dotted lines.

Bottom. Variance of individual cells (open symbols) and the mean ± SD (square, closed symbols) during baseline (-70 mV HP) and depolarization (-40 mV). Bsl variance is 22 ± 4.4 pA^2 and during the depolarization 22 ± 3.6 pA^2, n = 15 cells, $p > 0.05$.

G. Simultaneous, VC recording of Ca^{++} influx into a presynaptic varicosity (middle traces) and the PSCs in its postsynaptic partner (lower traces), without (**left**) or with (**right**) a 3-ms interval between the small and large presynaptic voltage pulses. The upper traces show the voltage waveforms applied. The suprathreshold depolarizations lasted 1.5 ms (left) and 3 ms (right).

H. Normalized preICa^{++} (**upper graph**) and PSC (**lower graph**) as a function of prepulse voltage for stimuli with (**right**) or without (**left**) a 3-ms interval between the prepulses and the suprathreshold depolarization.

Figure 4 legend.

A. Superimposed transmitted and fluorescence light pictures of the synaptically-connected MLI and postsynaptic Purkinje cell.

B. PSCs recorded from the Purkinje cell under two different experimental conditions: control (5 APs evoked in the MLI by depolarization to 0 mV from a HP of -60 mV at 33 Hz; black trace); test (same but with a 20 or 50 ms depolarization to -40 mV before the 1st AP; brown trace).

C. Ratio of the 1st PSC in test over control conditions: 1.25 ± 0.23 (mean ± SD, n = 8, $p < 0.05$).

D. Amplitudes of PSCs in a train normalized over the 1st PSC in control and test conditions. Data show the averages ± SD from 7 cells. Asteriks indicate statistical significance ($p < 0.05$).

E. Top. Superimposed transmitted and fluorescence light pictures highlighting the MLI axonal varicosity on top of the Purkinje cell soma. Same pair as in A. **Bottom.** Fluorescence light picture of the MLI. The inset shows the details of the recorded axonal varicosity. Yellow dotted lines show the approximate position of the recording pipette.

F. AxAPs recorded in the cell-attached configuration from the varicosity shown in **E** under the same experimental condition as in **B**. The inset shows an expanded view of the first axAPs in the train.

G. Ratio of the 1st AP widths (**Left**) and amplitudes (**Right**) in test over control conditions: mean width ± SD = 0.99 ± 0.09 (n = 12, $p > 0.05$); amplitude mean ± SD = 0.92 ± 0.06 (n = 12, $p < 0.05$).

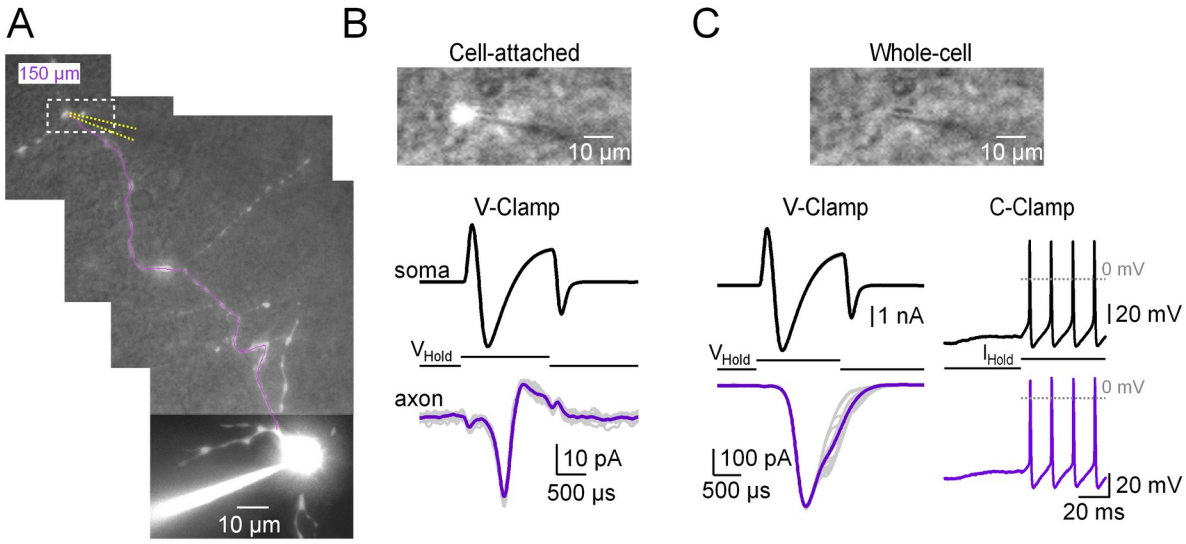
A
150 µm
10 µm
B
Cell-attached
10 µm
V-Clamp
soma
V_Hold
axon
10 pA
500 µs
C
Whole-cell
10 µm
V-Clamp
1 nA
V_Hold
100 pA
500 µs
C-Clamp
0 mV
20 mV
I_Hold
0 mV
20 mV
20 ms

Figure 1

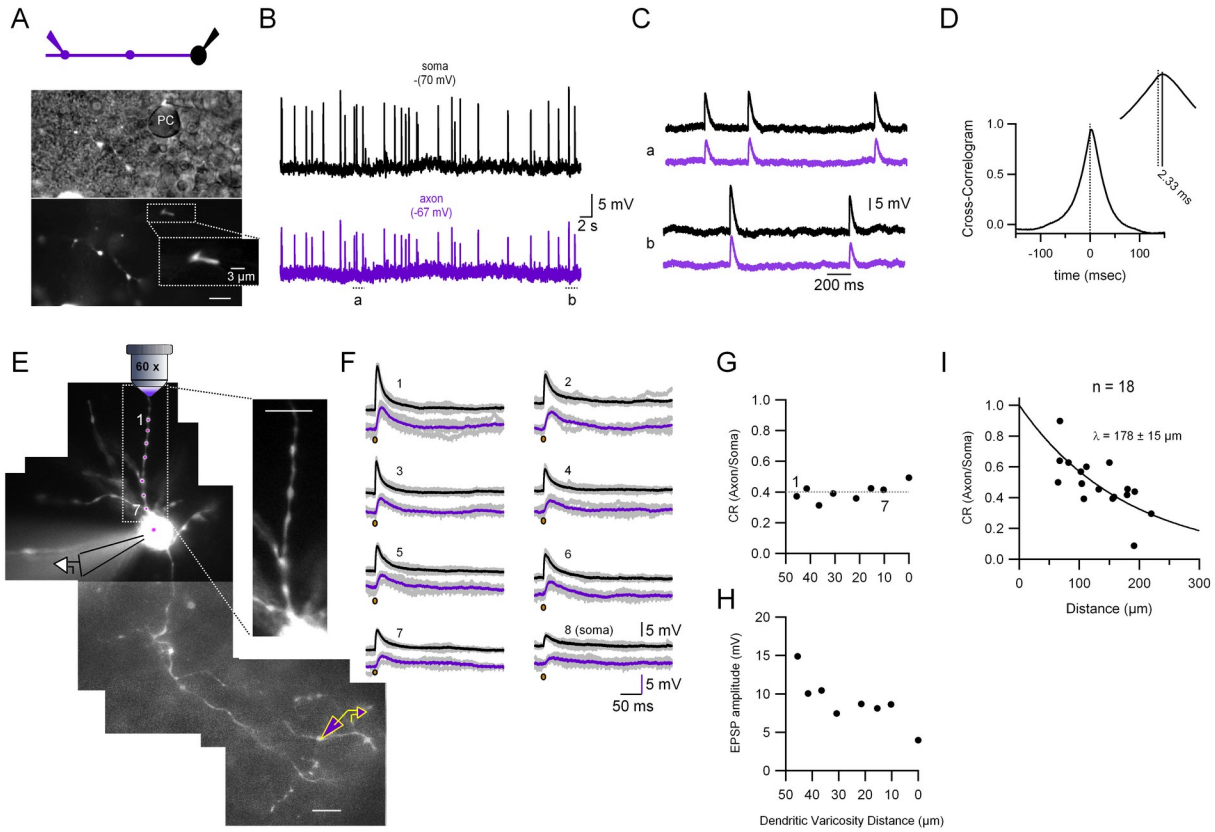
A
B
C
D
PC
3 µm
soma
-(70 mV)
axon
(-67 mV)
5 mV
2 s
a
b
5 mV
200 ms
Cross-Correlogram
1.0
0.5
0.0
-100
0
100
time (msec)
2.33 ms
E
60 x
1
7
F
1
2
3
4
5
6
7
8 (soma)
5 mV
5 mV
50 ms
G
CR (Axon/Soma)
1.0
0.8
0.6
0.4
0.2
0.0
1
7
50 40 30 20 10 0
H
EPSP amplitude (mV)
20
15
10
5
0
50 40 30 20 10 0
Dendritic Varicosity Distance (µm)
I
n = 18
λ = 178 ± 15 µm
CR (Axon/Soma)
1.0
0.8
0.6
0.4
0.2
0.0
0
100
200
300
Distance (µm)

Figure 2

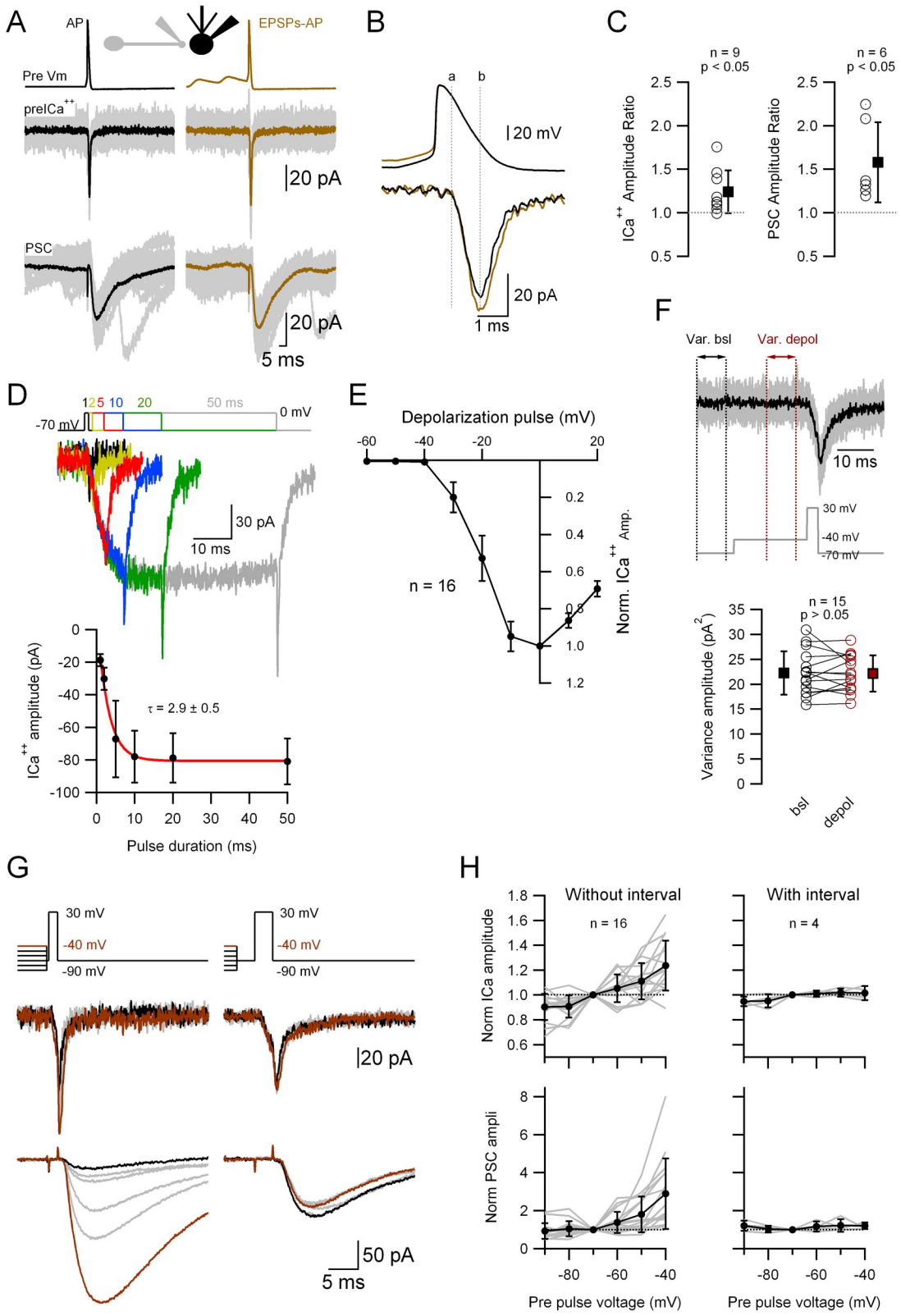
A
AP
EPSPs-AP
Pre Vm
preICa++
20 pA
PSC
20 pA
5 ms
B
a
b
20 mV
20 pA
1 ms
C
n = 9
p < 0.05
n = 6
p < 0.05
ICa++ Amplitude Ratio
PSC Amplitude Ratio
D
1 2 5 10 20 50 ms
-70 mV
0 mV
30 pA
10 ms
ICa++ amplitude (pA)
τ = 2.9 ± 0.5
Pulse duration (ms)
E
Depolarization pulse (mV)
n = 16
Norm. ICa++ Amp.
F
Var. bsl
Var. depol
10 ms
30 mV
-40 mV
-70 mV
n = 15
p > 0.05
Variance amplitude (pA2)
bsl
depol
G
30 mV
-40 mV
-90 mV
20 pA
50 pA
5 ms
H
Without interval
n = 16
With interval
n = 4
Norm ICa amplitude
Norm PSC ampli
Pre pulse voltage (mV)
Pre pulse voltage (mV)

Figure 3

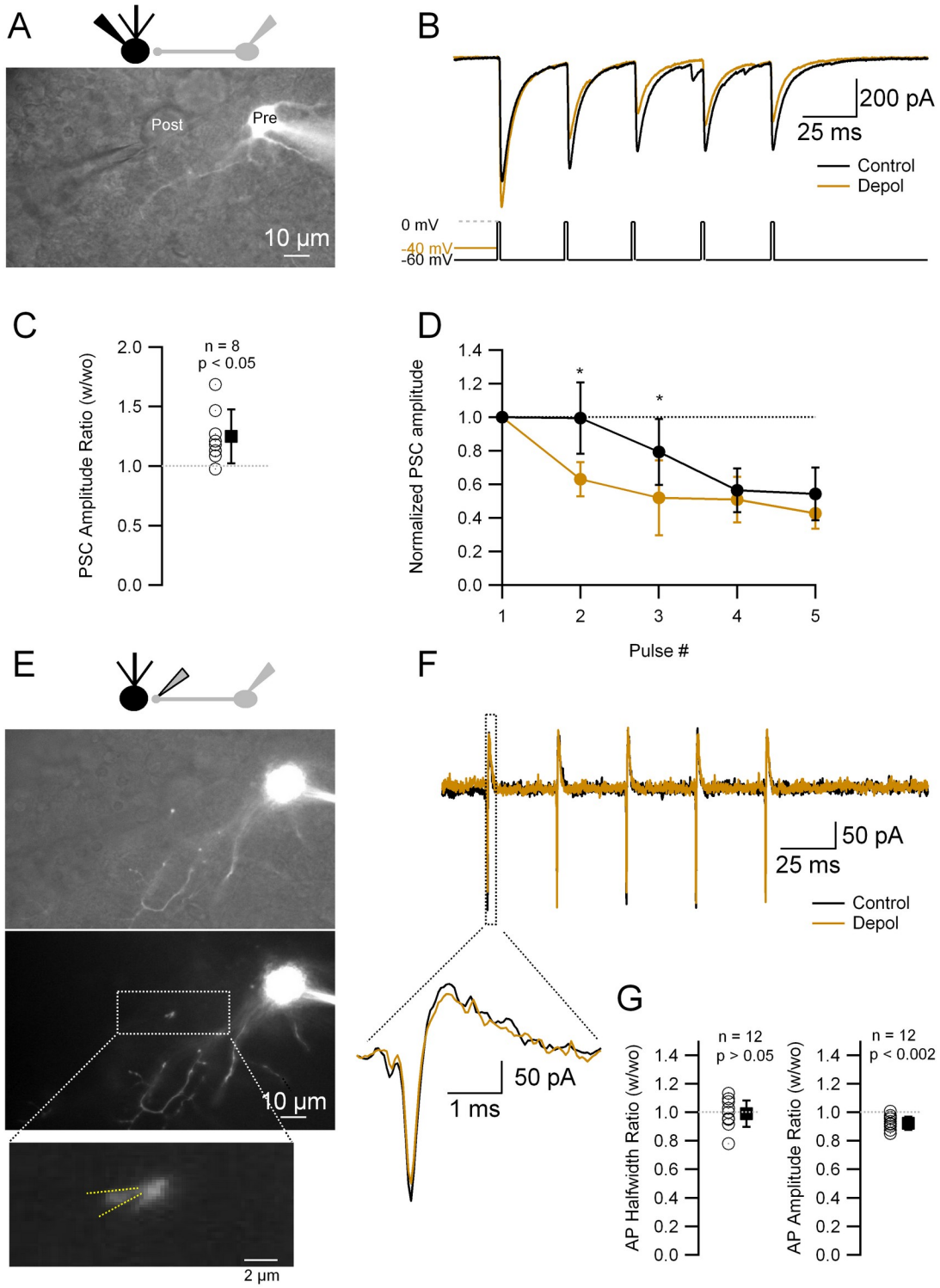
A
Post
Pre
10 µm
B
200 pA
25 ms
Control
Depol
0 mV
-40 mV
-60 mV
C
PSC Amplitude Ratio (w/wo)
n = 8
p < 0.05
D
Normalized PSC amplitude
Pulse #
E
10 µm
2 µm
F
50 pA
25 ms
Control
Depol
50 pA
1 ms
G
AP Halfwidth Ratio (w/wo)
n = 12
p > 0.05
AP Amplitude Ratio (w/wo)
n = 12
p < 0.002

Figure 4

Methods.

Preparation of cerebellar slices. Slices were prepared from Sprague-Dawley rats aged 12 to 37 days old. After decapitation, the cerebellum was quickly removed in an ice-cold extracellular solution (ES), the cerebellum taken out and sagittal cerebellar slices (202 µm width) cut with a Leica vibroslicer (VT1200S). The slices were kept in a recovering chamber at 34 ˚C until use. The composition of the ES was, in mM: NaCl 115, KCl 2.5, NaH_2PO_4 1.3, $NaHCO_3$ 26, Glucose 25, Na-pyruvate 5, $CaCl_2$ 2, $MgCl_2$ 1, pH 7.4 when bubbled with carbogen (95 % O_2 and 5 % CO_2). For animals aged 12 to 21 days the same afore-mentioned ES was used for the recordings. For animals aged above 21 days old a KGluconate-based ES was used for the dissection[32]; its composition (in mM): KGluconate 130, KCl 15, EGTA 0.05, Hepes 20, Glucose 25 and DAP5 50 µM, pH 7.4 and bubbled with carbogen.

Preparation of cerebellar cultures. The method for preparing primary dissociated cultures of cerebellar neurons was similar to that in a previous study[33]. Inhibitory interneurons were transfected with eGFP at 1 day after culture with adeno-associated virus (AAV) vector serotype 9 under the control of the CMV promoter. Interneurons could be visually identified from eGFP fluorescence. An axon of interneuron surrounding a PC soma was selected for whole-bouton recordings. Experiments were performed 3-5 weeks after preparation of the culture.

Electrophysiology. Both the soma and axon of MLIs were recorded with the patch-clamp technique[34] either in voltage or in current-clamp with a HEKA amplifier (EPC-10, double) and either Luigs & Neumann or Sutter manipulators. For the experiments presented in figures 1, 2 and 4 a KGluconate-based IS of the following composition (in mM) was used: 165 KGluconate, 10 HEPES, 1 EGTA, 0.1 $CaCl_2$, 4.6 $MgCl_2$, 4 Na_2ATP, 0.4 NaGTP, pH 7.3 and osmolarity 300 mOsm/KgH_2O. Alexa 594 (0.04 mM) was also added to the somatic recording pipette. With this IS the somatic pipettes had resistances of around 6 MΩ and the axonal ones 25 MΩ. To record the calcium currents (**figure 3**) a CsCl-based IS of the following composition (in mM) was used: 152 CsCl, 0.5 EGTA, 10 HEPES, 10.5 CsOH, 2 ATP, 0.2 GTP, pH 7.3 and osmolarity 300 mOsm/KgH_2O. With this IS the somatic pipettes had resistances of around 4 MΩ and the axonal ones 18 MΩ. In these experiments TEA (2 mM) and TTX (200 nM) were added to the extracellular solution in order to block K^+ and Na^+ voltage-dependent conductances.

Somatic and axonal pipettes were pulled with either HEKA (Pip 6) or Narishige (PP-83) vertical pullers. For experiments in the slice, we first recorded from the soma with the Alexa 594 containing IS. After a 5 to 10 minutes waiting time the fluorescence illumination was turned on in order to identify the axon and a suitab**References**le, superficial varicosity. In order to patch the axon a second pipette containing the KGluconate-based IS (without Alexa) was used. The axon was patched by looking at the image created by the camera with both the bright field and fluorescent lights on (**figures 1A** and **1B**). Pictures were taken at 1 Hz frequency in order to avoid photodamage.

Recordings in slices were done in an upright Olympus BX51W equipped with a 60×, 1.0 numerical aperture objective (NA). Experiments were done at near-physiological temperature (≈ 34 °C) with a Peltier system (Luigs & Neumann). Electrophysiological recordings from primary cultures were done in an inverted Olympus IX71 microscope equipped with a 40× objective (NA. 0.95). For experiments in slices, epifluorescence excitation was by light-emitting diode (LED) controlled by an OptoLED system (Cairn Research) at 572-/35-nm excitation and at 630/60 nm emission. Filters and dichroic were from Chroma Corporation (Vermont, USA). For experiments in cultures epifluorescence was by an LED light (Light Engine SOLA, Lumencore) at 450-/40nm excitation and 510-/50 nm emission; Fluorescent images were taken with Andor cameras (EMCCD Andor Ixon or a sCMOS Zyla 4.2).

Salts were either from Sigma Aldrich or Nacalai Tesque (Japan).

Photolysis. Glutamate was photolysed from MNI-Glutamate (4-Methoxy-7-nitroindolinyl-caged-L-glutamate; Tocris Biotechne, UK) with a 405 nm laser (Obis, Coherent, USA) following well-established procedures[17]. Briefly, MNI-Glutamate was added directly to the bath at a final concentration of 500 µM and photolysed with 100 to 200 µs and 1 to 3 mW laser pulses. Duration and power of the laser pulses were adjusted to obtain laser evoked EPSPs similar to spontaneous ones in terms of amplitude and time course. It is well known that laser power decreases exponentially with depth[17]. In order to be certain that the same amount of glutamate was released at each tested dendritic varicosity, only dendritic uncaging sites localized at the same imaging plane were chosen (see inset in **figure 2E**).

AP waveform.

The voltage waveforms used in the experiments presented in **figure 3A** (either the AP alone or the AP preceded by two EPSPs) were constructed from real AP and EPSPs recorded from an interneuron axonal varicosity; its width was 780 µs (see also **supplementary figure 1**) The resting Vm of the AP waveform is -70 mV and the peak of the AP is at 40 mV; the EPSPs interval is 19.5 ms, the EPSPs amplitude -58 (#1st EPSP) and -53 mV (2nd EPSP) and the duration of the depolarization (time between the onset of the EPSP and the onset of the AP) is 40 ms.

Analysis. EPSPs were detected using TaroTools extensions in IgorPro (https://sites.google.com/site/tarotoolsregister/), and the selection of each event was visually confirmed before subsequent analysis. The EPSPs coupling ratio, CR, represents the ratio of the peak axonal and peak somatic depolarizations.

The distance between the center of the soma and the recorded varicosity was measured offline from reconstructions of the recorded cell with Fiji[35]. The axonal AP widths and amplitudes (**figures 4** and **supplementary figure 1** and **4**) in cell-attached recordings were measured from peak to peak, which correspond to the maximal slopes of the rising and decaying phases of the AP voltage waveform.

Statistics. Data are presented as mean ± SD unless otherwise stated. Statistical significance was tested with the Wilcoxon signed-rank test for paired and the Wilcoxon-Mann-Whitney test for non-paired data. The difference between groups was considered significant when $p < 0.05$. In **supplementary figure 4** (axonal AP width and amplitude vs firing frequency), the correlation was assessed by the Spearman rank correlation test. In **supplementary figure 3**, statistical significance between the means of the different groups was assessed with the Tukey and Neuman Keuls post-hoc tests.

References.

1. Zbili, M. & Debanne, D. Past and Future of Analog-Digital Modulation of Synaptic Transmission. *Front. Cell. Neurosci.* **13**, (2019).
2. Alle, H. & Geiger, J. R. P. Combined Analog and Action Potential Coding in Hippocampal Mossy Fibers. *Science* **311**, 1290–1293 (2006).
3. Shu, Y., Hasenstaub, A., Duque, A., Yu, Y. & McCormick, D. A. Modulation of intracortical synaptic potentials by presynaptic somatic membrane potential. *Nature* **441**, 761–765 (2006).
4. Thome, C. *et al.* Synaptic entrainment of ectopic action potential generation in hippocampal pyramidal neurons. *J. Physiol. (Lond.)* **596**, 5237–5249 (2018).
5. Pouzat, C. & Marty, A. Somatic Recording of GABAergic Autoreceptor Current in Cerebellar Stellate and Basket Cells. *J. Neurosci.* **19**, 1675–1690 (1999).
6. Christie, J. M., Chiu, D. N. & Jahr, C. E. Ca(2+)-dependent enhancement of release by subthreshold somatic depolarization. *Nat Neurosci* **14**, 62–68 (2011).
7. Bouhours, B., Trigo, F. F. & Marty, A. Somatic Depolarization Enhances GABA Release in Cerebellar Interneurons via a Calcium/Protein Kinase C Pathway. *J. Neurosci.* **31**, 5804–5815 (2011).
8. Rowan, M. J. M., DelCanto, G., Yu, J. J., Kamasawa, N. & Christie, J. M. Synapse-Level Determination of Action Potential Duration by K(+) Channel Clustering in Axons. *Neuron* **91**, 370–383 (2016).
9. Rowan, M. J. M. & Christie, J. M. Rapid State-Dependent Alteration in Kv3 Channel Availability Drives Flexible Synaptic Signaling Dependent on Somatic Subthreshold Depolarization. *Cell Rep* **18**, 2018–2029 (2017).
10. Trigo, F. F. *et al.* Presynaptic miniature GABAergic currents in developing interneurons. *Neuron* **66**, 235–247 (2010).
11. Zorrilla de San Martin, J., Jalil, A. & Trigo, F. F. Impact of single-site axonal GABAergic synaptic events on cerebellar interneuron activity. *J. Gen. Physiol.* **146**, 477–493 (2015).
12. Southan, A. P. & Robertson, B. Patch-clamp recordings from cerebellar basket cell bodies and their presynaptic terminals reveal an asymmetric distribution of voltage-gated potassium channels. *J. Neurosci.* **18**, 948–955 (1998).

13. Southan, A. P., Morris, N. P., Stephens, G. J. & Robertson, B. Hyperpolarization-activated currents in presynaptic terminals of mouse cerebellar basket cells. *J. Physiol. (Lond.)* **526 Pt 1**, 91–97 (2000).
14. Southan, A. P. & Robertson, B. Electrophysiological characterization of voltage-gated K(+) currents in cerebellar basket and purkinje cells: Kv1 and Kv3 channel subfamilies are present in basket cell nerve terminals. *J. Neurosci.* **20**, 114–122 (2000).
15. Rall, W. Time constants and electrotonic length of membrane cylinders and neurons. *Biophys. J.* **9**, 1483–1508 (1969).
16. Canepari, M., Nelson, L., Papageorgiou, G., Corrie, J. E. T. & Ogden, D. Photochemical and pharmacological evaluation of 7-nitroindolinyl-and 4-methoxy-7-nitroindolinyl-amino acids as novel, fast caged neurotransmitters. *Journal of Neuroscience Methods* **112**, 29–42 (2001).
17. Trigo, F. F., Corrie, J. E. T. & Ogden, D. Laser photolysis of caged compounds at 405 nm: Photochemical advantages, localisation, phototoxicity and methods for calibration. *Journal of Neuroscience Methods* **180**, 9–21 (2009).
18. Katz, B. & Miledi, R. Membrane noise produced by acetylcholine. *Nature* **226**, 962–963 (1970).
19. Katz, B. & Miledi, R. Further observations on acetylcholine noise. *Nat New Biol* **232**, 124–126 (1971).
20. Geiger, J. R. & Jonas, P. Dynamic control of presynaptic Ca(2+) inflow by fast-inactivating K(+) channels in hippocampal mossy fiber boutons. *Neuron* **28**, 927–939 (2000).
21. Carta, M. *et al.* Membrane Lipids Tune Synaptic Transmission by Direct Modulation of Presynaptic Potassium Channels. *Neuron* **81**, 787–799 (2014).
22. Scott, R., Ruiz, A., Henneberger, C., Kullmann, D. M. & Rusakov, D. A. Analog modulation of mossy fiber transmission is uncoupled from changes in presynaptic Ca2+. *J. Neurosci.* **28**, 7765–7773 (2008).
23. Hering, S. *et al.* Calcium channel gating. *Pflugers Arch* **470**, 1291–1309 (2018).
24. Glitsch, M. & Marty, A. Presynaptic Effects of NMDA in Cerebellar Purkinje Cells and Interneurons. *J. Neurosci.* **19**, 511–519 (1999).

25. Blanchard, K., Zorrilla de San Martín, J., Marty, A., Llano, I. & Trigo, F. F. Differentially poised vesicles underlie fast and slow components of release at single synapses. *J. Gen. Physiol.* **152**, (2020).
26. Ritzau-Jost, A. *et al.* Large, Stable Spikes Exhibit Differential Broadening in Excitatory and Inhibitory Neocortical Boutons. *Cell Rep* **34**, (2021).
27. Kawaguchi, S. & Sakaba, T. Control of Inhibitory Synaptic Outputs by Low Excitability of Axon Terminals Revealed by Direct Recording. *Neuron* **85**, 1273–1288 (2015).
28. Kawaguchi, S.-Y. Dynamic Factors for Transmitter Release at Small Presynaptic Boutons Revealed by Direct Patch-Clamp Recordings. *Front Cell Neurosci* **13**, 269 (2019).
29. Vandael, D. *et al.* Subcellular patch-clamp techniques for single-bouton stimulation and simultaneous pre- and postsynaptic recording at cortical synapses. *Nat Protoc* **16**, 2947–2967 (2021).
30. Rowan, M. J. M., Tranquil, E. & Christie, J. M. Distinct Kv Channel Subtypes Contribute to Differences in Spike Signaling Properties in the Axon Initial Segment and Presynaptic Boutons of Cerebellar Interneurons. *J. Neurosci.* **34**, 6611–6623 (2014).
31. Begum, R., Bakiri, Y., Volynski, K. E. & Kullmann, D. M. Action potential broadening in a presynaptic channelopathy. *Nat Commun* **7**, 12102 (2016).
32. Blot, A. & Barbour, B. Ultra-rapid axon-axon ephaptic inhibition of cerebellar Purkinje cells by the pinceau. *Nat. Neurosci.* **17**, 289–295 (2014).
33. Kawaguchi, S. & Hirano, T. Sustained structural change of GABA(A) receptor-associated protein underlies long-term potentiation at inhibitory synapses on a cerebellar Purkinje neuron. *J. Neurosci.* **27**, 6788–6799 (2007).
34. Hamill, O. P., Marty, A., Neher, E., Sakmann, B. & Sigworth, F. J. Improved patch-clamp techniques for high-resolution current recording from cells and cell-free membrane patches. *Pflugers Arch.* **391**, 85–100 (1981).
35. Schindelin, J. *et al.* Fiji: an open-source platform for biological-image analysis. *Nat Methods* **9**, 676–682 (2012).